Check for updates

Carbothermal reduction of mill scales formed on steel billets during continuous casting

S. M. Espinoza Suarez[1] · L. E. Borja-Castro[1] · M. I. Valerio-Cuadros[1,2] ·
A. Bustamante Domínguez[1] · H. A. Cabrera-Tinoco[1,3] · E. Huaman[1] ·
R. A. Valencia-Bedregal[1] · Xiaoli Zhao[4] · Youyun Zhang[4] · Deliang Zhang[4] ·
C. H. W. Barnes[5] · L. De Los Santos Valladares[1,4,5]

Abstract

A billet is a bar made from crude steel which surface contains scales which are rich in iron oxides. This study presents the carbothermal reduction of the scales formed in steel billets. The process included the reaction of the iron oxides contents with carbon (in ratio 5:1) and annealing in a tubular furnace under argon atmosphere. The occurred reactions are discussed using thermodynamic calculations and thermal analysis which indicate a three-stage reduction process $Fe_3O_4 \rightarrow FeO \rightarrow Fe_3C \rightarrow \alpha$-Fe with intermediate reactions at the interval temperature 960 and 1300 °C. The X-ray diffraction confirms the reduction to α-Fe with minor presence of unreacted C, magnetite and wustite. Mössbauer spectroscopy analysis was performed at room temperature where a typical sextet corresponding to the dominant α-Fe is shown as well as wustite, magnetite and cementite to a lesser extent. The magnetization measurements confirm the ferromagnetic state corresponding to the α-Fe.

Keywords Mill scales · Steel billets · Continuous casting process · Steel industry · Mossbauer spectroscopy · Carbothermal reduction · X-ray diffraction

---

✉ L. De Los Santos Valladares
ld301@cam.ac.uk

[1] Laboratorio de Cerámicos y Nanomateriales, Facultad de Ciencias Físicas, Universidad Nacional Mayor de San Marcos, Ap. Postal 14-0149, Lima, Peru

[2] Departamento de Física, Universidade Estadual de Maringá, Av. Colombo, 5790 - Jardim Universitário, Maringá, PR 87020-900, Brazil

[3] Facultad de Ingeniería, Universidad Continental, 15311 Lima, Peru

[4] School of Materials Science and Engineering, Northeastern University, No 11, Lane 3, Wenhua Road, Heping District, Shenyang 110819, Liaoning, People's Republic of China

[5] Cavendish Laboratory, Department of Physics, University of Cambridge, J.J Thomson Ave, Cambridge CB3 0HE, UK

1 Introduction

Nowadays there is a high interest in metal recycling since this can offer a significant number of environmental benefits [1]. One of the last steps during steelmaking includes the injection the steel melt through a nozzle or hole located at the base of the ladle furnace. The steel passes through a continuous casting, formed by 4 casting lines through copper molds at around 1550 °C. The surface of the steel is then solidified through a process of cooling with water until it has a semi-product in the form of billets. During this process, iron ore fines, sponge iron fines and steel scale are released from the surface billets that are not used because they are very small particles. [2, 3].

Therefore, it is necessary to develop new advanced manufacturing techniques for the recycling of steel slag. This to improve the quality of life of low-income residents and preserve the environment. For recycling, the mill scales must be firstly reduced. There is not much information on mill steel scale reduction in the literature. However, it is possible to reduce its iron oxide components and it occurs from one phase to another, or even simultaneously. For example, the transformation from hematite to magnetite can occur in the same temperature range like from magnetite to wustite and followed by the reduction from wustite to metallic iron [4].

This work reports the carbothermal reduction of the mill scales formed on steel billets during continuous casting in SIDERPERU plant, Chimbote, Peru. This work responds to the problem of the loss of iron-bearing minerals in iron and steel wastes, which constitutes a problem to be faced by the steel industry. One of the causes is the limited efficiency of the metal separation process.

2 Experimental

2.1 Sample formation

The production process of the steelworks in SIDERPERU steel plant, Chimbote, Peru consists of several steps. One of the last steps includes the continuous casting of the melted steel. The steel previously obtained in a ladle furnace passes from a liquid to a solid phase. The molten steel is deposited into copper containers called ingot molds. These molds have squared section and are oscillating to avoid the sticking of steel on the walls. Billets are formed and come out continuously (continuous casting) with high pressure water injection to the 4 faces. This avoids the solidification of the center and prevents liquid from remaining during cutting. During the steel cooling by contact with environment and water, scales form on the billets surface which contain wustite, magnetite and hematite. These scales were collected and were crushed until the particle size ranged in the interval 53–600 μm. The powder was sieved by using a 72-μm sieve.

2.2 Carbothermal reduction

For carbothermal reduction, the samples were mixed with carbon in a ratio of 5:1 (50 g Iron oxide +10 g C) in a planetary ball milling machine for 6 h. Eventually, the mixing was heated at 1200 °C. The thermal treatment was performed in a tubular furnace in argon atmosphere. The temperature was set from room temperature (RT) and increased at 5 °C/

min to 500 °C, between 500 and 800 °C the heating speed was 10 °C/min. Then, the velocity between 800 to 1000 °C was set to 5 °C/min. The temperature was kept at 1000 °C for 1 h, then heating continued at 3 °C/min to reach 1140 °C and kept at this temperature for 1 h more. Then it was increased at 3 °C/min up to 1200 °C and kept at this temperature for 2 h. Eventually, the sample was quenched up to 300 °C with a speed of −10 °C/min. From 300 °C to room temperature, the speed was reduced to a rate of 3 °C/min at normal pressure.

2.3 Characterization

The thermal analysis was performed in a SETSYS18 TG-DTA-DSC equipment in an argon atmosphere from RT to 1300 °C under normal pressure. The heating rate was 10 °C/min. An alumina crucible (Al_2O_3) with 9.7 mg of sample and empty reference crucible for DSC was used. X-ray diffraction (XRD) measurements were taken in Rigaku diffractometers by using both, copper ($\lambda_{K\alpha}$ (Cu) = 1.54056 Å) and cobalt ($\lambda_{k\alpha}$ (Co) = 1.79026 Å) sources. The angle range were $20° \leq 2\theta \leq 80°$ and step 0.02°. Mössbauer spectroscopy (MS) measurement in transmission geometry were carried out using a ^{57}Co(Rh) source with 50 mCi of nominal activity. The spectrometer was calibrated and the determination of isomer shifts are given with respect to the a-Fe metal standard measured at room temperature. The spectra were obtained at room temperature. The isomer shift (δ), quadrupole splitting (ΔE_Q), and magnetic hyperfine field (B_{hf}), were obtained by a least-squares fitting routine using WinNormos program. The magnetic measurements were taken in a Quantum Design Inc. magnetometer (DC-MPMS-SQUID) with SQUID sensor in zero field cooling (ZFC) and field cooling (FC) modes. The magnetization as a function of temperature was recorded from 0 to 400 K applying a magnetic field of 500, 5000 and 10,000 Oe. The applied field dependence of the magnetization was obtained at 10, 110 and 300 K.

2.4 Calculation of the Gibbs free energy

The thermodynamic analysis were performed using the Shomate function [5]. This is a modified polynomial function of temperature to fit the curves of the enthalpy of formation and the standard entropy. The coefficients of these functions are specific for each compound and were extracted from the database of the National Institute of Standards and Technology (NIST) [6]. With these two thermodynamic quantities (enthalpy and entropy) we can calculate the Gibbs free energy through its definition ($\Delta G = \Delta H - T\Delta S$) and this is carried out for each chemical reaction here. The method mentioned above is a well-known procedure and the results are in accordance with those found in the literature [7, 8].

3 Results and discussion

Figure 1(a) shows the thermogram (TG – DTG/DSC) recorded during the carbothermal reduction of the mill steel scales. This was taken to understand better the reduction mechanism of the ferric oxide components. Figure 1(b) shows the DSC curve in the interval 960–1185 °C. The characteristic parameters of TG – DTG/DSC curve are listed in Table 1. The equipment traced the heating from RT to 1300 °C. The thermogravimetric (TG) curve, in Fig. 1(a) measures the mass loss as a function of the temperature. Note that the mass remains uniform from RT to 960 °C meaning that the sample is dry and does not contain water. However, above
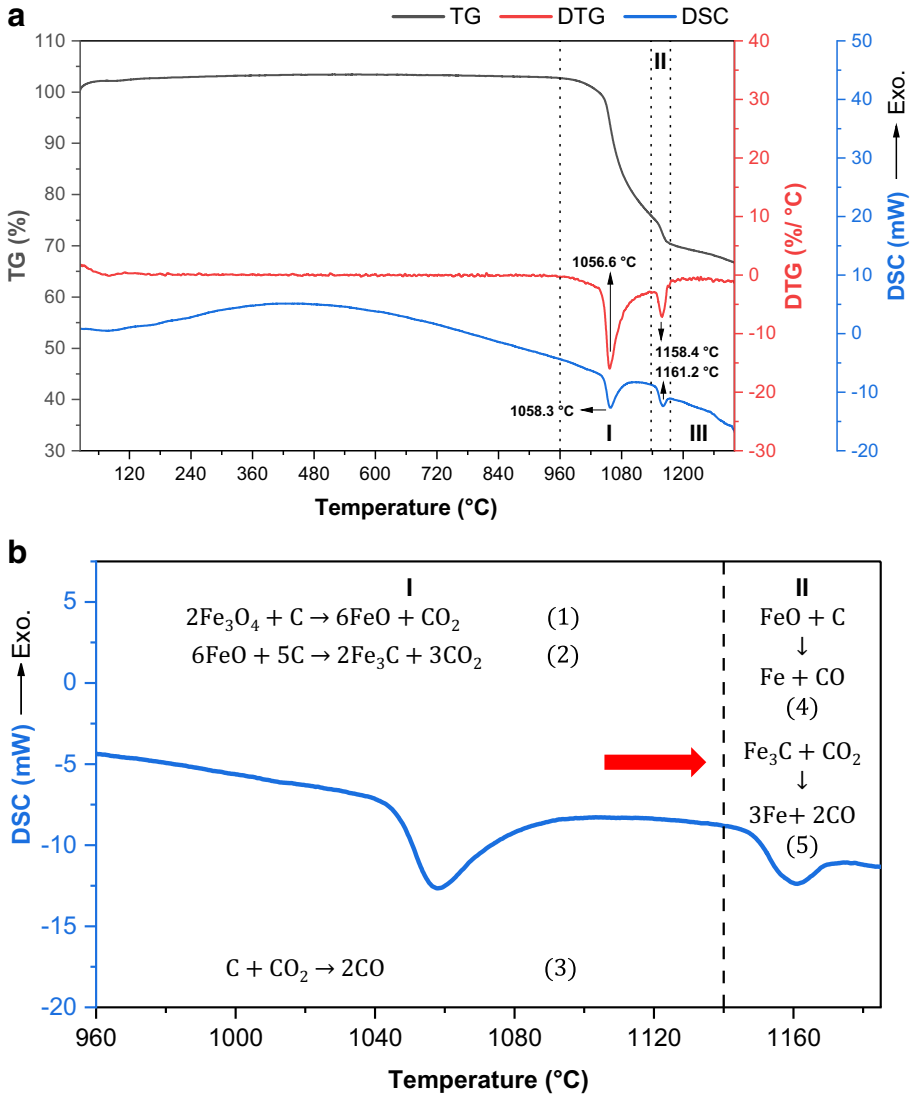
Fig. 1 **a** Thermogram (TG – DTG/DSC) and (**b**) zoomed DSC curve of the carbothermal reduction process of mill scales formed on steel billets. The most possible reaction equations are written per stage

Table 1 Thermal parameters obtained from TG – DTG/DSC curves during the carbothermal reduction process of mill scales formed on steel billets

Step	Temperature range (°C)	TG (%)	DTG Peak (°C)	DSC Peak (°C)
I	960–1140	27.20(3)	1056.6(4)	1058.3(4)
II	1140–1185	5.51(3)	1158.4(4)	1161.2(4)
III	1185–1300	3.31(1)	–	–
Total mass loss: 36.02(4) %				

	Temperature (975–1100) °C	Temperature (1101–1200) °C
Table 2 Possible reactions occurring during carbothermal reduction process of iron oxides between 975 and 1100 °C and 1101–1200 °C	Direct reduction	Direct reduction
	$6\,Fe_2O_3 + C \rightarrow 4\,Fe_3O_4 + CO_2$	$3\,Fe_2O_3 + C \rightarrow 2\,Fe_3O_4 + CO$
	$2\,Fe_3O_4 + C \rightarrow 6\,FeO + CO_2$	$Fe_3O_4 + C \rightarrow 3\,FeO + CO$
	$2\,FeO + C \rightarrow 2\,Fe + CO_2$	$FeO + C \rightarrow Fe + CO$
	Carbon gasification	Indirect reduction
	$C + CO_2 \rightarrow 2CO$	$3\,Fe_2O_3 + CO \rightarrow 2\,Fe_3O_4 + CO_2$
		$Fe_3O_4 + CO \rightarrow 3\,FeO + CO_2$
		$FeO + CO \rightarrow Fe + CO_2$

960 °C, three steps of mass loss are noted: 27.20(3) % (step I), 5.51(3) % (step II) and 3.31(1) % (step III). The total mass loss during heating was 36.02(4) %.

Before carbothermal reduction, the raw mill scales contained mainly wüstite (FeO), magnetite (Fe_3O_4), and a small amount of hematite (α-Fe_2O_3) [9]. In the present work, during the carbothermal reduction process, the first endothermic peak in the DSC plot corresponds to the solid-state reduction of the oxides with carbon through Eqs. (1) and (2) and as it is also indicated in Fig.1(b). Two reduction processes occur simultaneously at around 1058.3 °C: Reduction from Fe_3O_4 to FeO and reduction from FeO to Fe_3C (cementite). This process is accompanied with gasification of carbon via the Boudouard reaction which promotes the sudden mass loss through Eq. (3) [4, 10]. This reaction controls the overall process of the reduction.

The DSC curve also shows a second endothermic peak around 1161.2 °C. This should correspond to the direct reduction of the wüstite (previously obtained by reduction of the magnetite) with carbon to cementite through Eq. (4) [4]. This cementite reacts with carbon dioxide (generated in step I) following Eq. (5) [10]. In this step, fewer gases than in the previous step would be formed, which is reflected in a lesser mass loss.

Above 1185 °C no other reactions arise. However, because not all the components react with carbon gases there is still remaining cementite and carbon in the final product as confirmed by the XRD analysis below.

The reduction process can be carried out through various chemical reactions. Table 2 lists the possible reactions occurring during the reduction process in a blast furnace reported in the literature which we used as starting point for our analysis [11]. The reduction of the oxides occurs through interaction with graphite (direct) or through carbon monoxide formation (indirect). To elucidate which reactions are the most likely, the calculation of the Gibbs free energy and the enthalpy changes of the reactions was performed. The relationship of these thermodynamic quantities to temperature is shown in the Fig. 2.

The first stage of the reduction would correspond to the equations

$$2Fe_3O_4 + C \rightarrow 6FeO + CO_2 \tag{1}$$

$$6FeO + 5C \rightarrow 2Fe_3C + 3CO_2 \tag{2}$$

$$CO_2 + C \rightarrow 2CO \tag{3}$$
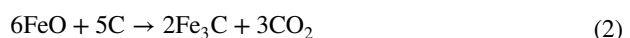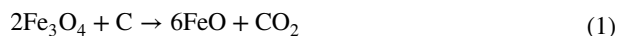
the reactions (1), (2) and (3) are exergonic at temperatures higher than 500 °C, 740 °C and 800 °C respectively, as can be seen in the Fig. 2a. It should be noted that the realization

Fig. 2 Gibbs free energies (a) and enthalpy changes (b) of the possible occurring during carbothermal reduction of iron oxides contained in mill scales
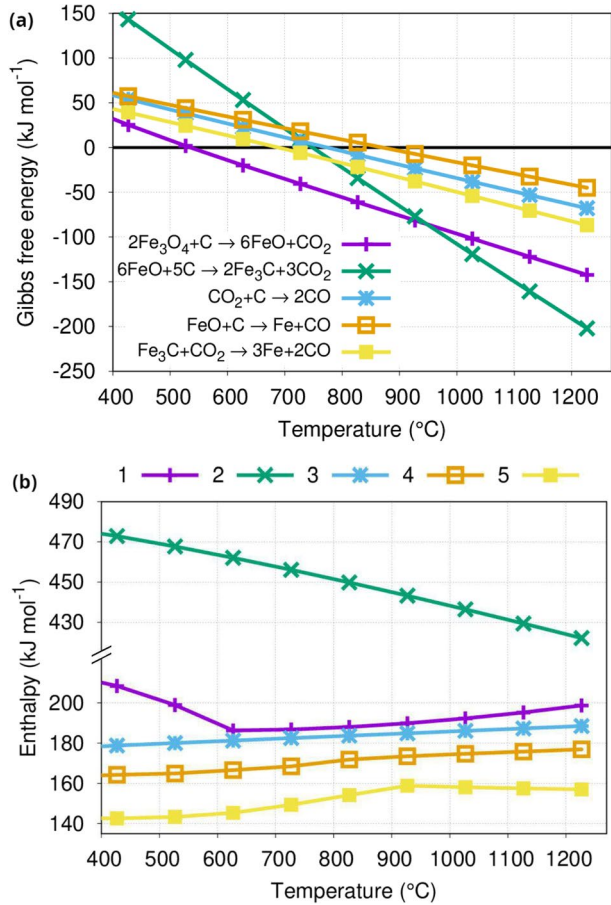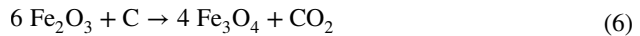

of the three equations would imply the generation of carbon monoxide and dioxide in the form of gases. This would result in a great loss of mass in the sample, which is in accordance with the DTG analysis (1056.6 °C). In addition, these three reactions are endothermic (see Fig. 2b), which would explain the first endothermic peak of the DSC analysis. At this point we must assume that the three equations are carried out simultaneously, causing that the first peak in the DSC curve to be larger than the second peak. The possibility that these reactions occur simultaneously is reported in the literature [12].

The second stage of the reduction process occurs through

$$FeO + C \rightarrow Fe + CO \tag{4}$$

$$Fe_3C + CO_2 \rightarrow 3Fe + 2CO \tag{5}$$

these reaction are spontaneous at temperatures above 900 °C and 700 °C, respectively (see Fig. 2a). It is observed from the Fig. 2b that the reactions are endothermic and that therefore it would correspond to the second endothermic peak of the DSC curve (1161.2 °C). In this reaction a mass loss of the sample is also expected but not to the same extent as in the reactions of the first stage. At the end of this stage, the recovery of iron is completed.
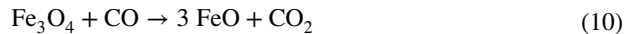
The reactions

$$6\,Fe_2O_3 + C \rightarrow 4\,Fe_3O_4 + CO_2 \tag{6}$$

$$3\,Fe_2O_3 + C \rightarrow 2\,Fe_3O_4 + CO \tag{7}$$

$$3\,Fe_2O_3 + CO \rightarrow 2\,Fe_3O_4 + CO_2 \tag{8}$$

are being disregarded in our procedure because it would involve an additional third stage in the reduction process, which is not observed in the DTG and DSC curves. Then

$$Fe_3O_4 + C \rightarrow 3\,FeO + CO \tag{9}$$

is exergonic in the temperature range of our scheme, but analysing the enthalpy change, the reaction (8) is as endothermic as the reaction (1). This should increase the area of the first peak on the DSC curve relative to the second peak even more than is observed. This makes the equation unlikely to occur but is not entirely discarded. A similar situation happens with the reaction

$$Fe_3O_4 + CO \rightarrow 3\,FeO + CO_2 \tag{10}$$

which is spontaneous but requires carbon monoxide to carry out. The analysis reported in the Ref. [9] indicates that magnetite is not the predominant phase. Therefore, it is estimated that when there is enough carbon monoxide for the reaction to occur, the magnetite must have already been reduced to wüstite. Finally, the reaction

$$FeO + CO \rightarrow Fe + CO_2 \tag{11}$$

is endergonic. This means that it is only possible if the concentration of carbon monoxide increases sufficiently in relation to the concentration of FeO and CO_2 [13], which cannot be stated with exactitude since the Eqs. (1), (2) and (3) produce both compounds. This would require a study of the gas concentration during the reduction process as in the case of Ref. [4].

It is important to take into account that the Fig. 2a poses only a lower limit for the temperature of the reactions. This temperature can be even higher by up to 200 °C depending on the rate of heating [14]. This would explain that some reactions could occur at higher temperatures, as is the case in the Eq. (1).

Figure 3 shows the XRD patterns (obtained with Cu and Co sources) of the reduced samples. The diffractograms detect α-Fe (PDF card No. 00–006-0696) and C (PDF card No. 00–001-0640) which demonstrate the reduction of the mill scale. Note that XRD obtained with Co radiation resolves better the Fe components than that of Cu radiation, since in contrast to Cu radiation, fluorescence due to ionization of the Fe atoms is prevented. In fact, the XRD taken with cobalt source also identifies Fe_3O_4, FeO, Fe_3C. The XRD in Fig. 3 are given in linear and logarithmic scales in order to reveal possible hidden peaks. On the right side the diffractogram is given with respect to the 2θ angle, whereas on the left side it is provided with respect to 2*d* displacement. The (110) and (200) crystallite sizes, obtained by using the Scherrer formula, were 85.6 and 92.4 nm, respectively. These values were obtained by performing the Rietveld refinement of the XRD obtained with Cu source (see *supplemental information*). Therefore, carbothermal reduction of iron oxide to α-Fe is demonstrated with both sources.
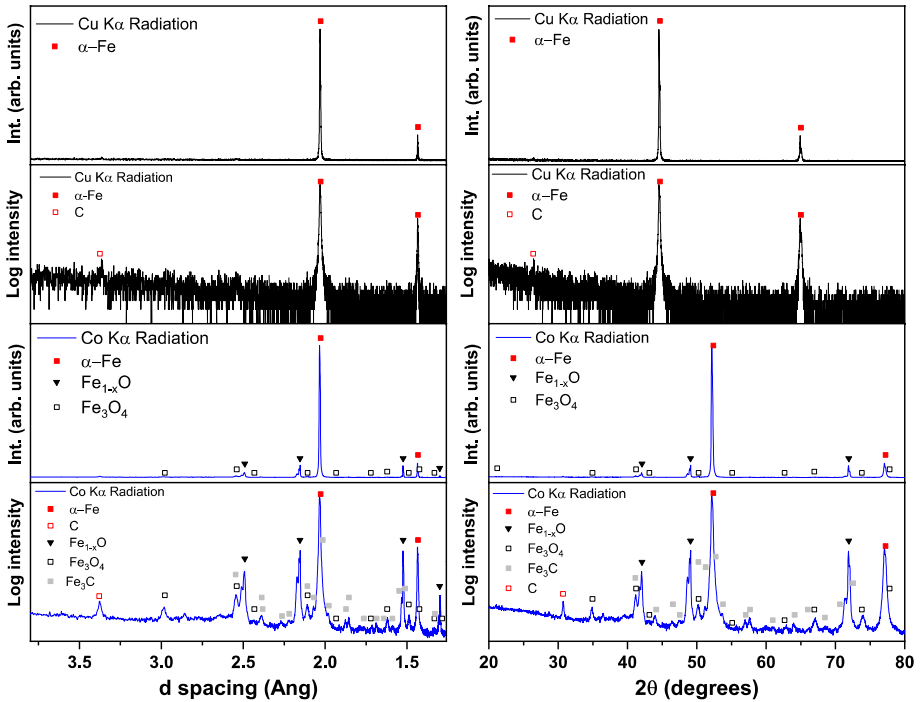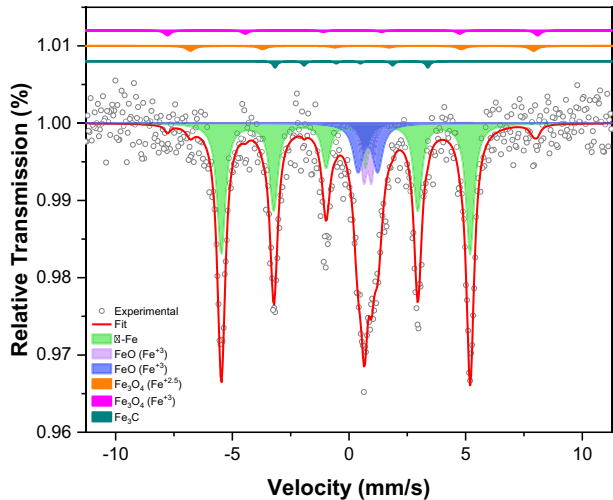
Fig. 3 Diffraction pattern for carbothermal reduced mill scales formed on steel billets in normal and logarithmical scales. Right: Angle scale (2θ). Left: d- spacing

**Fig. 4** Mössbauer spectrum for carbothermal reduced mill scales formed on steel billets

The Mössbauer spectrum obtained for the reduced sample at RT is shown in Fig. 4. The fitted parameters and the relative sub-spectral areas are given in Table 3. The spectrum was fitted with a discrete sextet corresponding to the α-Fe structure [15, 16]. Two doublets

Table 3 Mössbauer parameters of carbothermal reduced mill scales formed

Spectra	IS (mm/s)	QS (mm/s)	Bhf (T)	W (mm/s)	Area (%)
Alpha-Fe	−0.02(1)	–	33.1(2)	0.41(2)	69.5(1)
Wustite	0.90(2)	0.32(1)	–	0.3(3)	7.4(1)
	0.92(1)	0.85(2)	–	0.5(1)	18.4(1)
Magnetite	0.66(1)	0.0	45.5(2)	0.4(2)	2.5(1)
	0.26(2)	0.0	49.2(2)	0.3(2)	1.4(1)
Cementite	0.15(3)	0.13(1)	20.3(1)	0.2(1)	0.8(1)
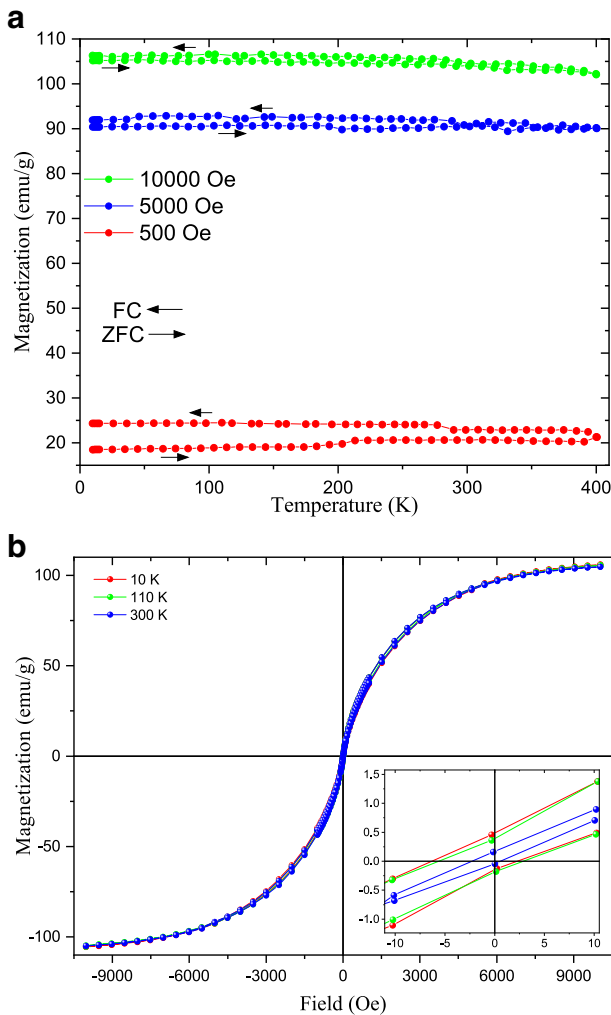
Fig. 5 Magnetic measurements. **a** Magnetization vs temperature obtained under 500, 5000 and 10,000 Oe applied fields. (**b**) Magnetization vs applied curves obtained at 10, 110 and 300 K

corresponding to Fe^{2+} and Fe^{3+} assigned to non-stochiometric wustite phases were revealed at RT [17, 18]. Two discrete sextets were adjusted with B_{hf} values of 49.2 and 45.5 T corresponding to the magnetite phase [19, 20]. The relative area ratio within Site B(Fe^{2+}) and Site A(Fe^{3+}) is 1.73 suggesting that is an oxidized magnetite. In addition, a discrete sextet with $B_{hf} = 20.3$ T phase was attributed to cementite structure [21, 22]. All phases revealed by the Mossbauer technic are in agreement with the X-ray diffraction result.

Figure 5(a) shows the magnetization as a function of the temperature curve (M(T)) under 500, 5000 and 10,000 Oe applied fields in the temperature range 5–400 K. No obvious magnetic transition is observed in the whole range of temperature. Instead, the curves are horizontal indicating ferromagnetic alignment belonging to α-Fe domains. No paramagnetic signal is detected over the whole interval of temperature demonstrating the complete reduction of the sample. In the figure, the magnetization values increase with applied field and the ZFC and FC loops become reversible since the spins increase alignment, typical from ferromagnetic materials.

In Fig. 5(b) the magnetization as a function of the applied (M (H)) curves are presented at 10, 110 and 300 K. At high applied fields the values of the magnetization remain constant, revealing ferromagnetic alignment of the domains. The presence of paramagnetic domains is discarded or might be minimal since the magnetization does not change with temperature. The magnetization behaviour at low applied fields is better observed in the inset figure, revealing a small hysteresis. It is visualized that decreasing the temperature, the coercivity and remanence increases, thus demonstrating the ferromagnetic behaviour of the sample.

4 Conclusions

Mill scales samples formed on steel billets during continuous casting have been carbothermally reduced. The initial samples were composed of wustite, magnetite and hematite. The thermogravimetric analysis showed three weight changes of 27.20(3)%, 5.51(3)% and 3.31(1)% between 960 and 1300 °C. Through thermal analysis and calculation of the Gibbs free energy and the enthalpy changes of the reactions, the carbothermal reduction process were assumed to include many reactions: Reduction of magnetite to wustite via $2Fe_3O_4 + C \rightarrow 6FeO + CO_2$ at approximately 500 °C, gasification of carbon ($CO_2 + C \rightarrow 2CO$) at 800 °C approximately and reduction of wustite to cementite ($2FeO + C \rightarrow 2Fe_3C + CO_2$) at 740 °C approximately in the first peak. Then reduction of wustite and cementite to α-Fe occurs via ($FeO + C \rightarrow Fe + CO$) at 900 °C, ($Fe_3C + C \rightarrow Fe + CO$) at 700 °C. Eventually, at around 1056.6 °C, a spontaneous reduction of wustite to alpha-iron occurs due to excess of wustite and carbon. The process is reflected in the DSC analysis which shows two endothermic peaks at 1058.3 and 1161.2 °C. Both, XRD and Mössbauer spectroscopy demonstrate the reduction of the iron oxides contained in the mill scales to α-Fe. This is also reflected in the magnetization measurements of the reduced sample where the ferromagnetic state belonging to the α-Fe domains is verified.

References

1. Corder, G.D., Golev, A., Giurco, D.: "Wealth from metal waste": translating global knowledge on industrial ecology to metals recycling in Australia. Miner. Eng. **76**, 2–9 (2015). https://doi.org/10.1016/j.mineng.2014.11.004
2. Ghosh, A., Chatterjee, A.: Ironmaking and Steelmaking: Theory and Practice. (2008)
3. Bhatta, G., De Los Santos Valladares, L., Liu, X., Ma, Z., Bustamante Domínguez, A.G., Moreno, N.O., Espinoza Suarez, S.M., Barnes, C.H.W., Zhang, D.: Microstructure and mechanical properties of solid state recycled 4Cr5MoSiV (H11) steel prepared by powder metallurgy. Results Mater. **10**, 100184 (2021). https://doi.org/10.1016/J.RINMA.2021.100184
4. Ubando, A.T., Chen, W.H., Ong, H.C.: Iron oxide reduction by graphite and torrefied biomass analyzed by TG-FTIR for mitigating CO2 emissions. Energy. **180**, 968–977 (2019). https://doi.org/10.1016/j.energy.2019.05.149
5. Shomate, C.H.: A Method for Evaluating and Correlating Thermodynamic Data, https://pubs.acs.org/doi/abs/10.1021/j150514a018, (1954)
6. Chase, J.M.W.: NIST-JANAF Themochemical tables-fourth edition. J. Phys. Chem. Ref. Data. monograph, 1–1951 (1998)
7. Treptow, R.S., Jean, L.: The Iron blast furnace: A study in chemical thermodynamics. J. Chem. Educ. **75**, 43 (1998). https://doi.org/10.1021/ed075p43
8. Mondal, K., Lorethova, H., Hippo, E., Wiltowski, T., Lalvani, S.B.: Reduction of iron oxide in carbon monoxide atmosphere—reaction controlled kinetics. Fuel Process. Technol. **86**, 33–47 (2004). https://doi.org/10.1016/j.fuproc.2003.12.009
9. Borja-Castro, L.E., Bustamante Domingues, A.G., Valerio-Cuadros, M.I.: Characterization of steel billet scales generated during the continuous casting process in SIDERPERU. (2021)
10. Sheshukov, O., Mikheenkov, M., Vedmi'd, L., Nekrasov, I., Egiazaryan, D.: Mechanism of ion-diffusion solid-phase reduction of Iron oxides of Technogenic origin in the presence of the liquid phase and without it. Metals (Basel). **10**, 1564 (2020). https://doi.org/10.3390/met10121564
11. Kawanari, M., Matsumoto, A., Ashida, R., Miura, K.: Enhancement of reduction rate of iron ore by utilizing iron ore/carbon composite consisting of fine iron ore particles and highly thermoplastic carbon material. ISIJ Int. **51**, 1227–1233 (2011). https://doi.org/10.2355/isijinternational.51.1227
12. Chen, Z., Dang, J., Hu, X., Yan, H.: Reduction kinetics of hematite powder in hydrogen atmosphere at moderate temperatures. Metals (Basel). **8**, (2018). https://doi.org/10.3390/met8100751
13. Treptow, R.S., Jean, L.: The iron blast furnace: A study in chemical thermodynamics. J. Chem. Educ. **75**, 43–47 (1998). https://doi.org/10.1021/ed075p43
14. Jozwiak, W.K., Kaczmarek, E., Maniecki, T.P., Ignaczak, W., Maniukiewicz, W.: Reduction behavior of iron oxides in hydrogen and carbon monoxide atmospheres. Appl. Catal. A Gen. **326**, 17–27 (2007). https://doi.org/10.1016/j.apcata.2007.03.021
15. Kramm, U.I., Ni, L., Wagner, S.: 57Fe Mössbauer spectroscopy characterization of Electrocatalysts. Adv. Mater. **31**, 1–11 (2019). https://doi.org/10.1002/adma.201805623
16. Stevens, J.G., Khasanov, A.M., Miller, J.W., Pollak, H.: Mossbauer Mineral Handbook. (2002)
17. Gheisari, M., Mozafari, M., Niyaifar, M., Amighian, J., Soleimani, R.: Observation of small exchange bias in defect wüstite (Fe 0.93O) nanoparticles. J. Supercond. Nov. Magn. **26**, 237–242 (2013). https://doi.org/10.1007/s10948-012-1821-9
18. Cho, S., Lee, J.: Metal recovery from stainless steel mill scale by microwave heating. Met. Mater. Int. **14**, 193–196 (2008). https://doi.org/10.3365/met.mat.2008.04.193
19. Vandenberghe, R.E., Barrero, C.A., Da Costa, G.M., Van San, E., De Grave, E.: Mössbauer characterization of iron oxides and (oxy)hydroxides: the present state of the art. Hyperfine Interact. **126**, 247–259 (2000). https://doi.org/10.1023/A:1012603603203
20. Doriguetto, A.C., Fernandes, N.G., Persiano, A.I.C., Nunes Filho, E., Grenèche, J.M., Fabris, J.D.: Characterization of a natural magnetite. Phys. Chem. Miner. **30**, 249–255 (2003). https://doi.org/10.1007/s00269-003-0310-x

21. Kniep, B., Constantinescu, A., Niemeier, D., Becker, K.D.: An in-situ Mössbauer study of the formation of cementite, Fe 3C. Zeitschrift fur Anorg. und Allg. Chemie. **629**, 1795–1804 (2003). https://doi.org/10.1002/zaac.200300136

22. Gangwar, A., Singh, A., Pal, S., Sinha, I., Meena, S.S., Prasad, N.K.: Magnetic nanocomposites of Fe3C or Ni-substituted (Fe3C/Fe3O4) with carbon for degradation of methylene orange and p-nitrophenol. J. Clean. Prod. **309**, 127372 (2021). https://doi.org/10.1016/j.jclepro.2021.127372